Steel and Composite Structures, *Vol. 28, No. 6 (2018) 735-748*
DOI: https://doi.org/10.12989/scs.2018.28.6.735

Free vibration analysis of functionally graded cylindrical shells with different shell theories using semi-analytical method

Majid Khayat *, Seyed Mehdi Dehghan [a],
Mohammad Amir Najafgholipour [b] and Abdolhossein Baghlani [c]

Department of Civil Engineering, Shiraz University of Technology, Shiraz, Iran

(*Received October 23, 2017, Revised June 9, 2018, Accepted July 7, 2018*)

Abstract. In this study, the semi-analytical finite strip method is adopted to examine the free vibration of cylindrical shells made up of functionally graded material. The properties of functionally graded shells are assumed to be temperature-dependent and vary continuously in the thickness direction according to a simple power law distribution in terms of the volume fraction of ceramic and metal. The material properties of the shells and stiffeners are assumed to be continuously graded in the thickness direction. Theoretical formulations based on the smeared stiffeners technique and the classical shell theory with first-order shear deformation theory which accounts for through thickness shear flexibility are employed. The finite strip method is applied to five different shell theories, namely, Donnell, Reissner, Sanders, Novozhilov, and Teng. The approximate procedure is compared favorably with three-dimensional finite elements. Finally, a detailed numerical study is carried out to bring out the effects of power-law index of the functional graded material, stiffeners, and geometry of the shells on the difference between various shell theories. Finally, the importance of choosing the shell theory in simulating the functionally graded cylindrical shells is addressed.

Keywords: free vibration; shell theories; FGM cylinder; stiffeners; finite strip method

1. Introduction

Functionally Graded Material (FGM) belongs to a class of advanced materials characterized by variation in properties as the dimension varies. Currently, FGMs have been widely applied in aerospace and nuclear industries. The overall properties of FGM are unique and different from any of the individual materials that form it. There is a wide range of applications for FGM which is expected to increase as the cost of material processing and fabrication processes are reduced. Pure metals are of little use in engineering applications because there are conflicting property requirements for different applications. For example, an application may require a material that is hard as well as ductile, but no such material exists in nature. To solve this problem, a combination (in molten state) of one metal with other metals or non-metals is used (Mahamood and Akinlabi 2012). As a new class of engineering materials, FGM has also been subjected to various types of studies including free vibration, linear and nonlinear buckling, and thermo-mechanical analyses (Farid *et al*. 2010, Jagtap *et al*. 2011, Khalili and Mohammadi 2012, Shahba and Rajasekaran 2012, Shahba *et al*. 2011, Chaht *et al*. 2015, Khayat *et al*. 2016a, b, 2017a, b, Mahmoud and Tounsi 2017). Many studies on the free vibration analysis of FGMs have been reported in the literature.

Various aspects of the dynamic behavior of composite materials such as laminated composite materials and FGM have been studied in many studies. Patel *et al*. (2005) researched the free vibration characteristics of functionally graded elliptical cylindrical shells using a higher-order theory through the thickness approximations of both in-plane and transverse displacements. The finite element employed in the study was based on field-consistency approach and free from shear and membrane locking problems. The strain–displacement relations were accurately introduced in the formulation without making any approximation in the thickness coordinate to radius ratio. Ganapathi (2007) studied the dynamic stability behavior of FGM spherical shells subjected to external pressure load. The material properties were graded in the thickness direction according to the power-law distribution in terms of volume fractions of the constituents of the material. The structural model was based on shear deformation theory and geometric non-linearity was considered in the formulation by using von Karman's assumptions. Nanda and Sahu (2012) analyzed the free vibration response of laminated composite shells with delamination using the finite element method based on first-order shear deformation theory. The shell theory used was the extension of a dynamic, shear deformable theory according to Sanders' first approximation for doubly curved shells, which can be reduced to Love and Donnell's theories by means of tracers. A dynamic analysis of doubly curved shell structures was conducted by Tornabene *et al*. (2014). The partial differential system of equations was solved by

*Corresponding author, Ph.D. Student,
E-mail: khayatmajid@yahoo.com
[a] Ph.D., Assistant Professor, E-mail: Dehghan@sutech.ac.ir
[b] Ph.D., Assistant Professor,
E-mail: Najafgholipour@sutech.ac.ir
[c] Ph.D., Associate Professor, E-mail: Baghlani@sutech.ac.ir

ISSN: 1229-9367 (Print), 1598-6233 (Online)

using the Generalized Differential Quadrature (GDQ) method. The paper focused on functionally graded doubly-curved shells and panels using various higher-order equivalent single layer theories and different through the thickness volume fraction distributions. Su *et al*. (2014) proposed a method for determining the natural frequencies of cylindrical, conical, and spherical shells with arbitrary subtended angle and general boundary conditions. The formulation was derived by the modified Fourier series in conjunction with Rayleigh-Ritz method according to the first-order shear deformation shell theory.

Many studies have been conducted concerning modeling and the effects of stiffeners on the behavior of different structures under various conditions; including among them, the following studies can be mentioned (Duc 2016, Rajasekaran 2013, Damnjanovic *et al*. 2017 and Qin *et al*. 2017).

Civalek (2017) solved the differential equations by the differential quadrature and discrete singular convolution methods. Governing equations of motion were obtained based on two different shell theories such as Love's shell theory and first-order shear deformation theory. Jin *et al*. (2015) presented a modified Fourier–Ritz approach for free vibration analysis of laminated functionally graded shallow shells with general boundary conditions in the framework of first-order shear deformation shallow shell theory. The displacement and rotation components of the shells were represented by the modified Fourier series consisting of standard Fourier cosine series and several closed-form auxiliary functions. Lee and Kwak (2015) used the Rayleigh–Ritz method to derive a dynamic model for the free vibration analysis of a circular cylindrical shell. The dynamic model was constructed according to Donnell's theory. Tornabene *et al*. (2015) compared the results obtained from the following methods: classical two-dimensional (2D) and three-dimensional (3D) finite elements (FEs), classical and refined 2D generalized differential quadrature (GDQ). Then they presented an exact three-dimensional solution for free vibration analysis of one-layered and multilayered composite shell panels. Vibration modes were investigated to make a comparison between the results obtained from the FE and GDQ methods (numerical solutions) and those obtained from the exact three-dimensional solution. Wali *et al*. (2015) studied the free vibration response of functionally graded material (FGM) shell structures using an efficient 3d-shell model based on a discrete double directors shell element. The mechanical properties of the shell structure were assumed to vary continuously in the thickness direction according to the general power-law distribution in terms of the volume fractions of the constituents. The fundamental equations for the FGM shell structures were derived using virtual work. Tornabene *et al*. (2016) presented a numerical procedure based on the Generalized Differential Quadrature (GDQ) method to solve the strong form of the differential equations that govern the free vibration problem of some structural elements. In semi-analytical finite strip method to approximate displacements and rotations in the direction in which geometry and material properties do not change, Fourier series are taken into account, while, in the other direction, the structure is discretized into several finite elements, which can be of low or high order types. One of the advantages of the finite strip method in comparison to other numerical methods is less number of degrees of freedom required for the analysis of shells without imperfection, so that the cost of analyzes is reduced and the speed of analysis increases.

The above review demonstrates that some literature exists on the vibration of functionally graded shells but most of it is restricted to a single shell theory. It should also be emphasized that most of previous studies did not indicate which shell theories have the best results for free vibration analysis. The present paper is concerned with the free vibration analysis of eccentrically stiffened functionally graded cylindrical shells. First, the fundamental equations for the free vibration analysis of stiffened shell segments were derived based on classical shell theory using the smeared stiffener technique and adjacent equilibrium criterion. The semi-analytical finite strip method was used to obtain the natural frequencies based on five different shell theories (Donnell 1934, Reissner 1941, Sanders 1959, Novozhilov 1964 and Teng and Hong 1998). The results were also compared with 3D finite element results referred to as exact solution. Semi-analytical numerical comparisons were carried out between different theories to explore their differences as well as similarities. Particular attention was paid to the effect of using a different set of linear strain–displacement relations on the predicted free vibration of eccentrically stiffened functionally graded cylindrical shells. Then, the effects of various parameters such as power-law index of functionally graded material, geometry of shell, and geometry of stiffeners on the vibration of the shells were discussed.

2. Theoretical development

2.1 Shell geometry and coordinate system

The position of a shell point is given by: θ as the circumferential coordinate, s as the meridional coordinate, and z as the coordinate normal to the middle surface which are shown in Figs. 1(a)-(b).

It should be noted that, owing to the weakness of composite material in shear stress, in this article, the first-order shear deformation theory has been utilized. Therefore, the displacement field corresponding to the first-order shear deformation theory is given as

$$\begin{aligned} \bar{u}(s,\theta,z) &= u(s,\theta) + z\beta_s(s,\theta) \\ \bar{v}(s,\theta,z) &= v(s,\theta) + z\beta_\theta(s,\theta) \\ \bar{w}(s,\theta,z) &= w(s,\theta) \end{aligned} \tag{1}$$

where, u, v and w are displacements in the middle plane of the laminate and β_s and β_θ are the rotations of the normal axis at the middle plane around the θ and s axes, respectively.

2.2 Functionally graded materials

It is assumed that the FGM cylindrical shell is made of a mixture of a metal phase (denoted by m) and a ceramic

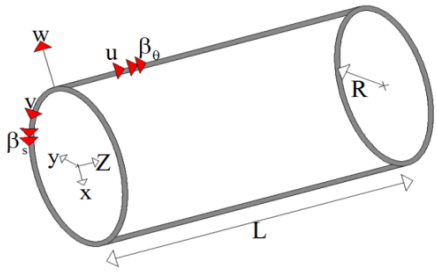

(a) 3D shell

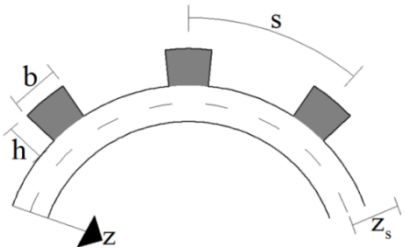

(b) Stringer stiffeners

Fig. 1 Geometry and coordinate system of stiffened FGM

phase (denoted by c), where the material composition varies only smoothly along its thickness direction. Thus, the materials properties of FGM, such as Young's modulus E or Poisson's ratio υ, can be expressed as (Sofiyev (2010)-Torki *et al*. (2014))

$$F_{eff}(z) = F_m V_m(z) + F_c V_c(z) \tag{2}$$

where F_{eff} is the effective mechanical or physical property and F_m and F_c are the material properties of metal and ceramic, respectively. z is the coordinate in the normal to the middle surface. Also, V_m and V_c stand for the volume fractions of metal and ceramic, respectively that are related by

$$V_m(z) + V_c(z) = 1 \tag{3}$$

The ceramic phase has a greater elasticity modulus, and lower density, and lower Poisson's ratio than the metal phase. V_m can be expressed by the power law

$$V_m = \left(\frac{z}{h} + \frac{1}{2}\right)^{Nfgm} \quad , Nfgm \geq 0 \tag{4}$$

where Nfgm is the power law exponent, which is a critical parameter in controlling the distribution of the constituents. If the effective elasticity modulus of FGM increases with Nfgm, the material is transformed into ceramic. Similarly, if the effective elasticity modulus of FGM decreases with Nfgm, the material is transformed into metal. In this study, the temperature has been assumed to be equal to the reference temperature (the environment temperature), i.e., 300 K. The equations used to estimate the effective material properties (the effective Young's modulus E_{eff}, the effective mass density ρ_{eff}, the effective Poisson's ratio v_{eff}, the effective shear modulus G_{eff}) are based on the power law distribution and can be expressed as

$$\begin{aligned}
E_{eff} &= (E_c - E_m)\left(\frac{z}{h} + \frac{1}{2}\right)^{Nfgm} + E_m \\
\rho_{eff} &= (\rho_c - \rho_m)\left(\frac{z}{h} + \frac{1}{2}\right)^{Nfgm} + \rho_m \\
\nu_{eff} &= (\nu_c - \nu_m)\left(\frac{z}{h} + \frac{1}{2}\right)^{Nfgm} + \nu_m \\
G_{eff} &= (G_c - G_m)\left(\frac{z}{h} + \frac{1}{2}\right)^{Nfgm} + G_m
\end{aligned} \tag{5}$$

2.3 Semi analytical method

In semi-analytical finite strip method, to approximate displacements and rotations in the direction in which geometry and material properties do not change, Fourier series are used, while, in the other direction, the structure is discretized into several finite elements which can be of low or high order types. In the present analysis the shell is divided into several closed strips with their nodal lines in the circumferential direction.

The circumferential variables of the global displacements (u, v, w, β_s, and β_θ) can be described by a suitable Fourier series expansion which generally consists of both symmetric and anti-symmetric terms as

$$\begin{aligned}
u(s,\theta,t) &= \left(u^{c_0}(s) + \sum_{n=1}^{NH}\left[u^{c_n}(s)\cos(n\theta) + u^{s_n}(s)\sin(n\theta)\right]\right)e^{-i\omega t} \\
v(s,\theta,t) &= \left(v^{c_0}(s) + \sum_{n=1}^{NH}\left[v^{c_n}(s)\cos(n\theta) + v^{s_n}(s)\sin(n\theta)\right]\right)e^{-i\omega t} \\
w(s,\theta,t) &= \left(w^{c_0}(s) + \sum_{n=1}^{NH}\left[w^{c_n}(s)\cos(n\theta) + w^{s_n}(s)\sin(n\theta)\right]\right)e^{-i\omega t} \\
\beta_s(s,\theta,t) &= \left(\beta_s^{c_0}(s) + \sum_{n=1}^{NH}\left[\beta_s^{c_n}(s)\cos(n\theta) + \beta_s^{s_n}(s)\sin(n\theta)\right]\right)e^{-i\omega t} \\
\beta_\theta(s,\theta,t) &= \left(\beta_\theta^{c_0}(s) + \sum_{n=1}^{NH}\left[\beta_\theta^{c_n}(s)\cos(n\theta) + \beta_\theta^{s_n}(s)\sin(n\theta)\right]\right)e^{-i\omega t}
\end{aligned} \tag{6}$$

where θ stands for the circumferential angular coordinate, n is the circumferential wave number, NH is the number of harmonic terms in the truncated series, and c_n and s_n are coefficients of Fourier series.

2.4 Comparison with other theories for general thin shells

The strains in an arbitrary point of shell thickness and with distance z from mid-surface can be expressed in terms of mid-surface strains ε_{ss}, $\varepsilon_{\theta\theta}$ and $\gamma_{s\theta}$ and also mid-surface changes of curvatures κ_{ss}, $\kappa_{\theta\theta}$ and $\kappa_{s\theta}$.

$$\bar{\varepsilon}_{ss} = \varepsilon_{ss} + z\kappa_{ss} \qquad \bar{\varepsilon}_{\theta\theta} = \varepsilon_{\theta\theta} + z\kappa_{\theta\theta} \qquad \bar{\gamma}_{s\theta} = \gamma_{s\theta} + z\kappa_{s\theta} \tag{7}$$

The generalized strain vector is as follows

$$\varepsilon = \{\varepsilon_{ss}\ \varepsilon_{\theta\theta}\ \gamma_{s\theta}\ \kappa_{ss}\ \kappa_{\theta\theta}\ \kappa_{s\theta}\ \gamma_{\theta z}\ \gamma_{sz}\} \tag{8}$$

where linear strain-displacement relations are (Teng and Hong 1998)

$$\varepsilon_{ss}=\frac{\partial u}{\partial s}\quad \varepsilon_{\theta\theta}=\frac{1}{R}\frac{\partial v}{\partial\theta}+\frac{w}{R}\quad \gamma_{s\theta}=\frac{\partial v}{\partial s}+\frac{1}{R}\frac{\partial u}{\partial\theta} \tag{9}$$

moreover, the transverse shear strains can be calculated as follows

$$\gamma_{sz}=\beta_s+\beta_{ss}\qquad \gamma_{\theta z}=\beta_\theta+\beta_{\theta\theta} \tag{10}$$

The semi-analytical method is used to obtain the natural frequencies based on five different shell theories (Donnell, Reissner, Sanders, Novozhilov, and Teng). Differences between different linear strain–displacement relations are only found in the expressions of curvatures, twisting curvature, and the transverse shear strains (Teng and Hong 1998). The differences are highlighted in Table 1.

The vector of stress resultants is defined as

$$\sigma=\{N_{ss}\ \ N_{\theta\theta}\ N_{s\theta}\ M_{ss}\ \ M_{\theta\theta}\ \ M_{s\theta}\ Q_{sz}\ Q_{\theta z}\}^T \tag{11}$$

N_{ss}, $N_{\theta\theta}$ and $N_{s\theta}$ are the in-plane meridional, circumferential, and shearing force resultants per unit length, respectively. M_{ss}, $M_{\theta\theta}$ and $M_{s\theta}$ are the analogous couples, while Q_{sz} and $Q_{s\theta}$ are the transverse shear force resultants per unit length. The constitutive equation relates internal stress resultants and couples to generalized strain components on the middle surface.

$$\begin{Bmatrix} N_{ss}\\ N_{\theta\theta}\\ N_{s\theta}\\ M_{ss}\\ M_{\theta\theta}\\ M_{s\theta}\\ Q_{sz}\\ Q_{\theta z}\end{Bmatrix}=\begin{bmatrix} A_{11} & A_{12} & A_{16} & B_{11} & B_{12} & B_{16} & 0 & 0\\ A_{12} & A_{22} & A_{26} & B_{12} & B_{22} & B_{26} & 0 & 0\\ A_{16} & A_{26} & A_{66} & B_{16} & B_{26} & B_{66} & 0 & 0\\ B_{11} & B_{12} & B_{16} & D_{11} & D_{12} & D_{16} & 0 & 0\\ B_{12} & B_{22} & B_{26} & D_{12} & D_{22} & D_{26} & 0 & 0\\ B_{16} & B_{26} & B_{66} & D_{16} & D_{26} & D_{66} & 0 & 0\\ 0 & 0 & 0 & 0 & 0 & 0 & A_{44} & A_{45}\\ 0 & 0 & 0 & 0 & 0 & 0 & A_{45} & A_{55}\end{bmatrix}\begin{Bmatrix} \varepsilon_{ss}\\ \varepsilon_{\theta\theta}\\ \gamma_{s\theta}\\ k_{ss}\\ k_{\theta\theta}\\ k_{s\theta}\\ \gamma_{sz}\\ \gamma_{\theta z}\end{Bmatrix} \tag{12}$$

A_{ij} is extensional stiffness, D_{ij} is bending stiffness, and B_{ij} is bending-extensional coupling stiffness (Torki *et al.* 2014) and are defined as

$$\begin{aligned} A_{11}&=A_{22}=\frac{E_1}{1-\upsilon^2}+\frac{E_sA_s}{s} & A_{12}&=\frac{E_1\upsilon}{1-\upsilon^2}\\ A_{66}&=\frac{E_1}{2(1+\upsilon)}\\ B_{11}&=B_{22}=\frac{E_2}{1-\upsilon^2}+C & B_{12}&=\frac{E_2\upsilon}{1-\upsilon^2}\\ B_{66}&=\frac{E_2}{2(1+\upsilon)}\\ D_{11}&=D_{22}=\frac{E_3}{1-\upsilon^2}+\frac{E_sI_s}{s} & D_{12}&=\frac{E_3\upsilon}{1-\upsilon^2}\\ D_{66}&=\frac{E_3}{2(1+\upsilon)}\\ A_{44}&=A_{55}=K_s\frac{E_1}{2(1+\upsilon)}\end{aligned} \tag{13}$$

with

$$\begin{aligned} E_1&=(E_m+\frac{E_c-E_m}{Nfgm+1})h\\ E_2&=\frac{(E_c-E_m)h^2}{2(Nfgm+1)(Nfgm+2)}\\ E_3&=[\frac{E_m}{12}+(E_c-E_m)(\frac{1}{Nfgm+3}-\frac{1}{Nfgm+2}\\ &+\frac{1}{4Nfgm+4})]h^3\end{aligned} \tag{14}$$

And the local stiffness of the stiffener is

$$C=\frac{E_sA_sz_s}{s} \tag{15}$$

In Eqs. (13), (14), and (15), E_s is the elastic modulus in the axial direction of the corresponding stiffener, the spacing of the stiffeners is denoted by s, the quantities of A_s are the cross section areas of the stiffeners, and I_s are the second moments of cross section areas and, z_s are eccentricities of the stiffeners with respect to the middle surface of the shell. K_s is the shear correction factor.

Table 1 Comparison of curvatures and twisting curvature

Theory	$\boldsymbol{\beta_{ss}}$	$\boldsymbol{\beta_{\theta\theta}}$	$\boldsymbol{\beta_n}$	$\boldsymbol{\beta_m}$	$\boldsymbol{\kappa_{ss}}$	$\boldsymbol{\kappa_{\theta\theta}}$	$\boldsymbol{\kappa_{s\theta}}$
Donnell	$\frac{\partial w}{\partial s}$	$-\frac{1}{R}\frac{\partial w}{\partial\theta}$			$\frac{\partial\beta_s}{\partial s}$	$\frac{\partial\beta_\theta}{R\partial\theta}$	$\frac{\partial\beta_\theta}{\partial s}+\frac{\partial\beta_s}{\partial\theta}$
Reissner	$-\frac{\partial w}{\partial s}$	$\frac{v}{R}-\frac{1}{R}\frac{\partial w}{\partial\theta}$			$\frac{\partial\beta_s}{\partial s}$	$\frac{\partial\beta_\theta}{R\partial\theta}$	$\frac{\partial\beta_\theta}{\partial s}+\frac{\partial\beta_s}{\partial\theta}-\beta_s$
Novozhilov	$-\frac{\partial w}{\partial s}$	$\frac{v}{R}-\frac{1}{R}\frac{\partial w}{\partial\theta}$		$\frac{\partial u}{R\partial\theta}$	$\frac{\partial\beta_s}{\partial s}$	$\frac{\partial\beta_\theta}{R\partial\theta}$	$\frac{\partial\beta_\theta}{\partial s}+\frac{\partial\beta_s}{\partial\theta}-\beta_\theta+\frac{\beta_m}{R}$
Sanders	$-\frac{\partial w}{\partial s}$	$\frac{v}{R}-\frac{1}{R}\frac{\partial w}{\partial\theta}$	$\frac{v}{2R}$		$\frac{\partial\beta_s}{\partial s}$	$\frac{\partial\beta_\theta}{R\partial\theta}$	$\frac{\partial\beta_\theta}{\partial s}+\frac{\partial\beta_s}{\partial\theta}-\beta_\theta+\frac{\beta_n}{R}$
Teng	$-\frac{\partial w}{\partial s}$	$\frac{v}{R}-\frac{1}{R}\frac{\partial w}{\partial\theta}$			$\frac{\partial\beta_s}{\partial s}$	$\frac{\partial\beta_\theta}{R\partial\theta}$	$\frac{\partial\beta_\theta}{\partial s}+\frac{\partial\beta_s}{\partial\theta}-\beta_\theta$

The equations of motion with the related boundary conditions can be obtained by using the Hamilton principle, which is expressed as

$$\int_{t_1}^{t_2} (\delta T - \delta U)\, dt = 0 \tag{16}$$

where t_1 and t_2 are two arbitrary times, δ is the variational operator, T and U are the kinetic and potential energies of the FGM shell, respectively. The virtual work of the internal forces, including the nonzero initial stresses, can be obtained from the variations of the shell elastic potential energy as

$$\delta U = \int_{\varphi}\int_{\theta}\int_{z} \begin{pmatrix} \sigma_{ss}\delta\varepsilon_{ss} + \sigma_{\theta\theta}\delta\varepsilon_{\theta\theta} + \tau_{s\theta}\delta\gamma_{s\theta} \\ +\tau_{sz}\delta\gamma_{sz} + \tau_{\theta z}\delta\gamma_{\theta z} \end{pmatrix} R dz d\theta d\varphi \tag{17}$$

By taking the integral of Eq. (17) in the thickness direction and by using Eq. (12), the internal virtual work can be written as

$$\begin{aligned} \delta W_{int}^{L} = & \int_{0}^{l_o}\int_{0}^{2\pi} (N_{ss}\delta\varepsilon_{ss} + N_{\theta\theta}\delta\varepsilon_{\theta\theta} + N_{s\theta}\delta\gamma_{s\theta} \\ & + M_{ss}\delta k_{ss} + M_{\theta\theta}\delta k_{\theta\theta} + M_{s\theta}\delta k_{s\theta} \\ & + Q_{ss}\delta\gamma_{ss} + Q_{\theta\theta}\delta\gamma_{\theta\theta}) R d\theta ds \end{aligned} \tag{18}$$

in which l_o is the length of shell generator. Discretization of δU by using Eq. (18) gives

$$\delta W_{int}^{L} = \sum_{j=1}^{nstrip} (\delta\Delta_j)^T K_{ej} \Delta_j \tag{19}$$

in this equation, Δ_j contains all unknown coefficients of displacements and rotations of jth strip and $\delta\Delta_j$ represents its virtual counterpart, also K_{ej} is the linear stiffness matrix of jth strip. For the variation of total kinetic energy

$$\delta T = \int_{V} \rho_{eq}(z)[\ddot{u}\,\delta u + \ddot{v}\delta v + \ddot{w}\delta w] \tag{20}$$

or

$$\begin{aligned} \delta T = & \int_{A} [I_0(\dot{u}\,\delta u + \dot{v}\,\delta v + \dot{w}\delta w) + I_1(\dot{\beta}_s\delta u + \dot{u}\,\delta\beta_s \\ & + \dot{\beta}_\theta\delta v + \dot{v}\delta\beta_\theta) + I_2(\dot{\beta}_s\delta\beta_s + \dot{\beta}_\theta\delta\beta_\theta)] \end{aligned} \tag{21}$$

where

$$\rho_{eq} = \rho_{eff}(z) + \left(\frac{A_s}{I_s h}\right)\rho_s \tag{22}$$

and

$$I_i = \int_{-h/2}^{h/2} \rho_{eq}(z)\, z^i dz, \qquad i = 0,1,2 \tag{23}$$

ρ_s is the density of isotropic stiffeners. The global stiffness and mass matrices of the stiffened shell structure (K, M) are achieved by assembling the stiffness and mass matrices of the shell and stiffener elements. Consequently, the following eigenvalue problem is obtained for the stiffened shell structure with natural frequency of ω.

$$(K - \omega^2 M)\, U = 0 \tag{24}$$

3. Results and discussion

In this section, some results and considerations concerning the free vibration problem of the FGM shells are presented. Based on the presented formulations, a computer program has been prepared in MATLAB to compute the global matrix and solve eigen-problems for free vibration. To verify the accuracy of the present method, some comparisons with available data in the literature have been performed.

3.1 Verification of solution method

3.1.1 FGM cylindrical shell

In order to demonstrate the accuracy of the present semi-analytical approach, Table 2 compares the free vibrations of functionally graded simply supported cylindrical shells with the results given by Patel *et al.* (2005) and Loy *et al*. (1999). The results have been calculated by Sanders's theory in the two studies. It was assumed that FGM shells were made of a mixture of zirconium (ZrO2) and titanium (Ti-6Al-4V). The material

Table 2 Comparison of natural frequencies in (Hz) for simply supported functionally graded circular cylindrical shells (h = 0.002 m, R/h = 500, L/R = 20)

	Nfgm = 0.5			Nfgm = 1			Nfgm = 5		
Harmonic Number (n)	Loy (1999)	Patel (2005)	Present study	Loy (1999)	Patel (2005)	Present study	Loy (1999)	Patel (2005)	Present study
2	4.517	4.520	4.490	4.480	4.484	4.461	4.407	4.410	4.389
4	7.097	7.100	7.071	7.038	7.041	7.028	6.926	6.928	6.910
6	16.594	16.605	16.574	16.445	16.466	16.448	16.192	16.203	16.176
8	30.023	30.062	30.003	29.771	29.811	29.800	29.296	29.334	29.272
10	47.301	47.339	47.313	46.905	46.943	46.930	46.155	46.193	46.133

Table 3 Material properties of the FGM cylindrical shell

Elastic modulus of metal E_m (GPa)	Elastic modulus of ceramic E_c (GPa)	Density of metal ρ_m (Kg/m^3)	Density of ceramic ρ_c (Kg/m^3)	Poisson's ratio of metal v_m	Poisson's ratio of ceramic v_c
207.788	205.098	8166	8900	0.317756	0.31

properties are listed in Table 3.

It is clear that the results of the present method are in in good agreement with those of Loy (1999) and Patel (2005). The maximum relative error is about 2.76%.

3.1.2 Isotropic stiffened cylindrical shell

In this section, the free vibration analysis is carried out for cylindrical shells having two fixed ends (F-F) and simple ends (S-S). The material properties and geometry of the shell are summarized in Table 4 according to Naghsh *et al*. (2015).

Table 5 shows the natural frequencies of the un-stiffened cylinder and those of cylinders stiffened with 16 concentric and eccentric stringers. The results have been calculated by Reissner's theory in the two studies.

It can be concluded from Table 5 that the maximum difference between the results of the current study and those of Naghsh *et al*. (2015) is limited to 1.8% for the case of no-stringer, 1.86% for the case of exterior stringer, and 1.76% for the case of interior stringer. One reason for the observed difference between the results of these two studies is that Naghsh *et al*. (2015) used Lagrange polynomials to interpolate the displacement variables for both the circumferential and meridian directions of the shell element. In addition, stringer stiffeners were modeled as discrete curved beams to investigate the free vibration of stiffened shells.

3.2 Cylindrical shells

In this study, the effects of various parameters such as geometries and material properties on natural frequencies of cylindrical shell have been investigated. The properties of constituents, including the Young's modulus and Poisson's ratio are given in Table 6. The boundary conditions are pined-pined and radius of the shell is 304.875 mm.

Table 4 Mechanical and geometrical properties of the cylindrical shell with equally spaced stringers

L = 394.46 mm	R = 49.76 mm	h = 1.651 mm	E = 68.95 GPa
ρ = 2760 Kg/m^3	v = 0.3	h = 5.334 mm	b = 3.175 mm

3.2.1 Unstiffened cylindrical shells

In this section of the problem, the effects of different thicknesses on natural frequency obtained by different shell theories are investigated. The natural frequencies for the first ten modes have been presented in Table 7(a)-(c).

It appears that the difference between the results obtained from different variation shell theories increases with the increase of thickness. As can be observed from the results in Table 7, Novozhilov and Donnell shell theories gave the lowest and largest values, respectively. The difference between the results may be due to the different deformation simulation accuracy of different shell theories.

Table 6 Mechanical properties of nickel and alumina

Material	E (GPa)	υ	ρ (Kg/m^3)
Nickel	380	0.31	3800
Alumina	70	0.338	2702

Fig. 2 Three dimensional mesh elements of the cylindrical shell

Table 5 The first four natural frequencies of the cylinder with 16 stringers in (Hz)

Boundary condition	Stringer type	ω_1		ω_2		ω_3		ω_4	
		Naghsh (2015)	Present study	Naghsh (2015)	Present study	Naghsh (2015)	Present study	Naghsh (2015)	Present study
S-S	No-stringer	702	696	1272.00	1262	1489	1478	1641	1626
	Exterior stringer	703	696	1093.00	1083	1421	1404	1671	1641
	Interior stringer	605	599	1026.00	1016	1359	1339	1373	1361
F–F	No-stringer	1150	1129	1367.00	1354	1922	1889	2316	2297
	Exterior stringer	1157	1149	1248.00	1226	2023	2004	2024	2012
	Interior stringer	969	960	1109.00	1090	1606	1595	1906	1875

Table 7 The effects of different thicknesses on natural frequencies obtained by different shell theories (Nfgm = 10, L/R = 3)

(a) h = 0.183 mm

Mode	Donnell	Reissner	Sanders	Novozhilov	Teng
1	37.745	37.340	37.183	37.040	37.083
2	38.669	38.233	38.090	37.923	38.008
3	44.171	43.581	43.477	43.307	43.415
4	44.616	44.014	43.907	43.728	43.826
5	53.742	53.000	52.858	52.581	52.778
6	60.573	59.707	59.561	59.227	59.440
7	65.028	64.085	63.942	63.386	63.773
8	78.001	76.800	76.620	75.964	76.488
9	92.449	91.016	90.767	89.821	90.486
10	92.516	90.969	90.703	89.861	90.328

(b) h = 2.439 mm

Mode	Donnell	Reissner	Sanders	Novozhilov	Teng
1	63.136	63.136	63.136	63.136	62.505
2	66.862	66.862	66.862	66.862	65.525
3	75.284	75.284	75.284	75.284	73.026
4	93.502	93.502	93.502	93.502	89.762
5	96.701	96.701	96.701	96.701	91.866
6	123.967	123.967	123.967	123.967	116.529
7	153.901	153.901	153.901	153.901	143.128
8	155.801	155.801	155.801	155.801	143.337
9	191.736	191.736	191.736	191.736	174.480
10	231.591	231.591	231.591	231.591	208.432

(c) h = 4.878 mm

Mode	Donnell	Reissner	Sanders	Novozhilov	Teng
1	85.132	83.870	83.691	83.244	83.467
2	97.665	96.134	96.003	94.841	95.327
3	104.024	102.227	102.068	100.903	101.001
4	140.631	137.974	137.824	136.118	136.116
5	153.866	150.938	150.791	148.387	149.529
6	187.905	184.164	183.721	180.737	182.229
7	243.542	238.405	237.904	233.778	235.690
8	275.455	269.618	268.412	263.757	266.280
9	306.762	299.949	297.891	291.759	294.825
10	377.227	368.838	365.944	358.679	362.312

Also the difference between natural frequencies obtained by different shell theories for higher modes is more than that of lower modes. With the aim of determining the accuracy of different theories, a number of analyses have been conducted by finite element software ABAQUS using around 39500 eight-nodded C3D8R solid elements with fine mesh (Fig. 2). In order to analyze the shells using three-dimensional element of ABAQUS software, shell is

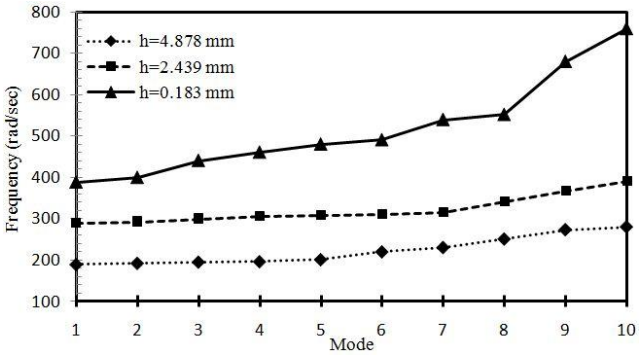

(a)

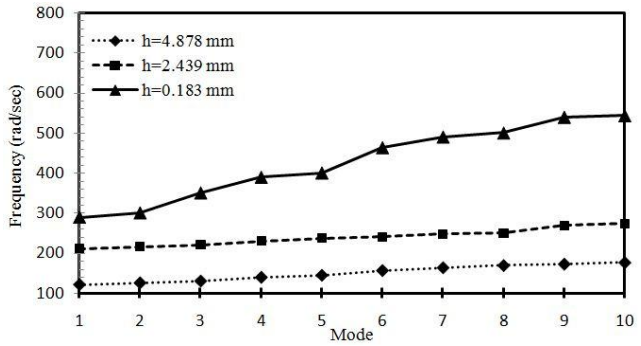

(b)

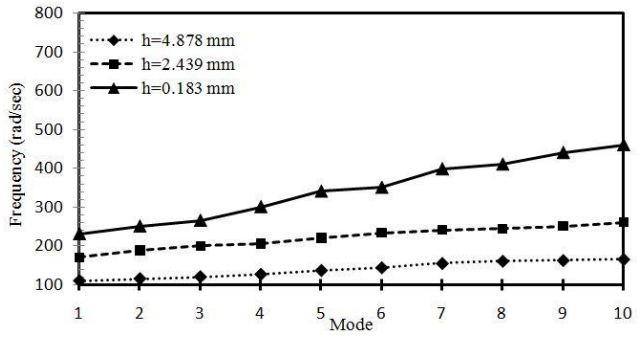

(c)

Fig. 3 The effect of thickness and Nfgms: (a) Nfgm = 0; (b) Nfgm = 5; (c) Nfgm = 30

Table 8 Comparison of the tenth frequency obtained by different theories and 3D solid elements for various thicknesses (mm)

Thickness	Donnell	Reissner	Sanders	Novozhilov	Teng	ABAQUS(3D)
0.183	92.516	90.969	90.703	89.861	90.328	90.682
2.439	231.591	231.591	231.591	231.591	208.432	231.582
4.878	377.227	368.838	365.944	358.679	362.312	364.790

Table 9 The effect of length-to-radius ratio on natural frequencies obtained by different shell theories

(a) $L/R = 1$

Mode	Donnell	Reissner	Sanders	Novozhilov	Teng
1	229.614	223.481	222.306	220.884	221.316
2	238.521	231.910	230.739	228.277	229.245
3	244.632	237.712	236.327	233.580	234.916
4	267.125	259.423	257.781	254.054	256.132
5	286.076	277.182	275.597	272.041	274.064
6	310.641	300.676	298.911	294.851	296.998
7	356.909	345.284	342.640	337.978	340.998
8	365.403	353.476	349.848	345.492	348.258
9	429.125	415.011	410.702	405.583	408.514
10	463.162	447.697	443.121	437.610	440.088

(b) $L/R = 3$

Mode	Donnell	Reissner	Sanders	Novozhilov	Teng
1	69.935	68.067	67.604	66.794	66.927
2	76.885	74.754	74.201	73.425	73.433
3	88.396	85.895	85.152	84.330	84.417
4	119.792	116.315	115.035	113.648	113.902
5	120.860	117.103	115.909	114.544	114.820
6	162.072	156.810	154.863	153.486	153.781
7	210.407	203.554	201.995	199.049	199.428
8	214.746	207.736	204.706	202.866	202.952
9	265.332	256.287	252.344	249.673	249.964
10	326.621	315.349	310.466	304.841	306.997

(c) $L/R = 6$

Mode	Donnell	Reissner	Sanders	Novozhilov	Teng
1	40.296	39.083	38.596	38.171	38.384
2	54.351	52.624	52.016	51.423	51.719
3	54.533	52.773	52.168	51.549	51.858
4	82.116	79.409	78.510	77.553	78.031
5	112.655	108.928	107.165	106.035	106.600
6	117.616	113.532	111.873	110.567	111.220
7	159.895	154.304	151.464	149.603	150.534
8	187.577	180.942	177.502	175.247	176.375
9	187.577	180.481	177.153	175.048	176.101
10	187.577	180.276	176.560	174.433	175.497

meshed to the appropriate number in three directions: longitudinal, circumferential and thickness. In the direction of thickness, the shell is divided into at least 2400 solid elements so that constant properties can be attributed to each element. The tenth mode has the highest difference in the results of Table 7 As a result, a comparison of the results of this mode with those obtained from ABAQUS software has been presented in Table 8.

According to Table 8, it can be observed that the frequency values obtained from Sanders's theory have the maximum conformity with the values obtained from 3D analysis, and in comparison with the other shell theories studied in this research, they have a higher precision in the free vibration analysis of cylindrical shells.

In this part of the study, the effects of thickness on natural frequency for different modes in the clamped-clamped FGM cylindrical shell have been investigated by using Sanders's theory. In addition, three different thicknesses of 0.183, 2.439, and 4.878 mm and three different Nfgms of 0, 5, and 30 have been considered. The radius and length of the cylinder are 190.5 mm.

When the thickness varies from 0.183 to 4.878 mm, as shown in different parts of Figs. 3(a)-(c), the values of natural frequencies decrease in a similar way, as is the case for pure isotropic (Nfgm = 0) and FGM shells. The effect of length-to-radius ratio on the results of various theories is demonstrated in different parts of Tables 9(a)-(c) for h = 4.878 mm and Nfgm = 5.

It can be seen that the deeper the cylindrical shell, the higher the difference between the results obtained by different shell theories. It appears that the value of the natural frequency obtained by Donnell and Sanders's theories has the highest and lowest sensitivity to length-to-radius ratio, respectively. With the aim of validating the accuracy of different theories, a number of analyses have been conducted by the help of finite element software ABAQUS using solid elements. The tenth mode has the highest difference in the results of Table 9 As a result, a comparison of the results of this mode with those obtained from ABAQUS software has been presented in Table 10.

According to Table 10, it can be observed that the frequency values obtained from Sanders and Teng's theories have the maximum conformity with the values obtained from 3D analysis, and compared to the other shell theories studied in this research, they have a higher precision in the free vibration analysis of cylindrical shells.

In the next section, the effects of length-to-radius ratio on natural frequency of cylindrical shells with different Nfgms will be investigated. The results achieved by using Sanders's theory have been presented for different length-to-radius ratios which are 1, 3, 6 as well as different Nfgms

Table 10 Comparison of the tenth frequency obtained by different theories and 3D solid elements for various length to radius ratios (L/R)

L/R	Donnell	Reissner	Sanders	Novozhilov	Teng	ABAQUS(3D)
1	463.162	447.697	443.121	437.610	440.088	442.009
3	326.621	315.349	310.466	304.841	306.997	308.517
6	187.577	180.276	176.560	174.433	175.497	176.181

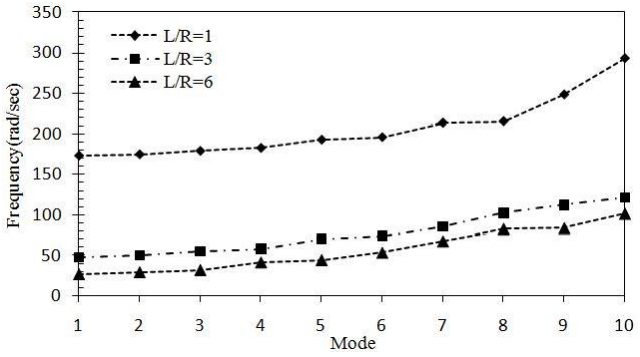

(a)

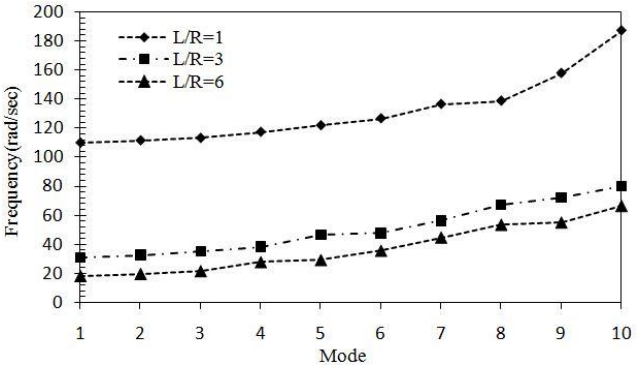

(b)

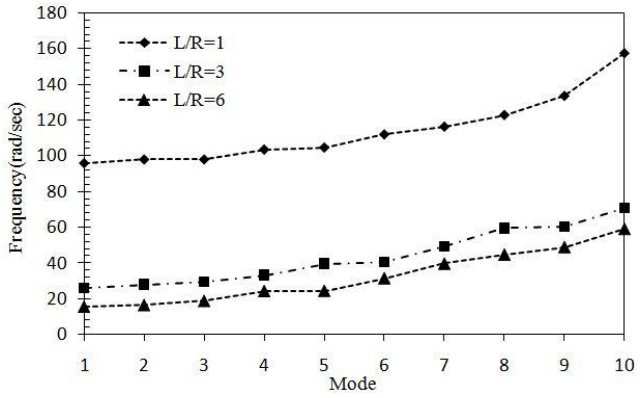

(c)

Fig. 4 The effect of length to radius ratio on frequencies: (a) Nfgm = 0; (b) Nfgm = 5; (c) Nfgm = 30

= 0, 5 and 30. The effects of length to radius ratio on increasing or decreasing the frequency are shown in Figs. 4(a)-(c).

Hence, it is concluded from Fig. 5 that the shell frequency reduces when the length to radius ratio increases and this is the case for all of the considered modes. However, this reduction does not have a significant relation with the increase of length-to-radius ratio. Moreover, the

Table 11 The effect of Nfgm on natural frequencies obtained by different shell theories

(a) Nfgm = 0

Mode	Donnell	Reissner	Sanders	Novozhilov	Teng
1	47.195	46.770	46.674	46.624	46.624
2	49.438	48.988	48.889	48.815	48.825
3	54.125	53.633	53.525	53.439	53.454
4	57.827	57.296	57.133	57.093	57.104
5	70.092	69.448	69.237	69.195	69.216
6	73.510	72.826	72.584	72.554	72.584
7	85.034	84.240	83.962	83.928	83.954
8	102.112	101.142	100.785	100.775	100.805
9	111.869	110.805	110.403	110.403	110.435
10	121.086	119.923	119.500	119.488	119.524

(b) Nfgm = 5

Mode	Donnell	Reissner	Sanders	Novozhilov	Teng
1	30.602	30.209	30.138	29.587	29.921
2	32.273	31.855	31.757	31.152	31.485
3	34.897	34.412	34.336	33.682	34.023
4	37.910	37.334	37.188	36.583	36.818
5	46.041	45.271	45.061	44.421	44.573
6	47.325	46.482	46.161	45.608	45.747
7	55.905	54.871	54.331	53.781	53.908
8	67.160	65.734	65.089	64.607	64.628
9	72.115	70.268	69.795	69.226	69.382
10	79.655	77.294	76.854	76.331	76.549

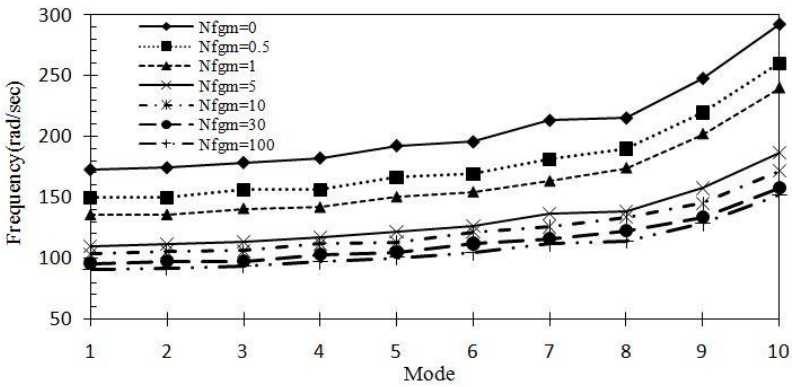

Fig. 5 The effect of Nfgm on natural frequencies of FGM

Table 11 Continued

(c) Nfgm = 30

Mode	Donnell	Reissner	Sanders	Novozhilov	Teng
1	26.314	25.637	25.436	25.298	25.380
2	28.182	27.383	27.163	27.084	27.110
3	29.546	28.682	28.374	28.327	28.375
4	33.393	32.394	32.052	31.928	31.991
5	39.745	38.485	38.079	37.933	38.016
6	40.709	39.410	38.880	38.740	38.799
7	49.507	47.923	47.266	47.048	47.065
8	59.514	57.607	56.691	56.451	56.543
9	60.369	58.403	57.502	57.208	57.345
10	70.607	68.306	67.251	66.910	67.007

variation trend of the shell frequency with changes in the thickness is approximately identical with the trend of different Nfgms.

The effect of the power-law index on the different results of various theories is demonstrated in Tables 11(a)-(c) for h = 0.813 mm and L/R = 1.

The frequency variation increases as Nfgm increases in various theories. This indicates the sensitivity of various theories to the power-law index, so that, the maximum sensitivity to Nfgm belongs to Novozhilov's theory, while Donnell's theory has the least sensitivity to it. In Table 12, the results calculated by the semi-analytical method according to the five theories, are compared with an analysis done by finite element software ABAQUS.

It can be observed in Table 12 that the frequency values obtained from Sanders and Teng's theories have the maximum conformity with the values obtained from 3D analysis, and compared to the other shell theories studied in this research, they are more precise in the free vibration analysis of cylindrical shells. In the next section, the effects of Nfgm on natural frequency for the ratio of L/R = 1 and h = 0.813 mm will be investigated. The results have been presented in Fig. 5.

As can be seen in Fig. 5, when Nfgm increases, the values of natural frequencies decrease and this is the same for all modes. Of course it does not have a certain ratio for different thicknesses.

In general, according to the obtained results, it can be concluded that changing of thickness, Nfgm, and length to radius ratio have the maximum effects, respectively, on the difference among the frequencies obtained from the five discussed theories.

Table 13 The effect of boundary conditions on natural frequencies obtained from different shell theories

(a) Fixed-free

Nfgm	Donnell	Reissner	Sanders	Novozhilov	Teng	ABAQUS
0	25.898	24.771	23.551	22.242	20.980	-
0.5	22.415	21.388	20.259	19.123	17.909	19.831
1	20.426	19.406	18.303	17.210	16.063	-
5	16.975	16.106	15.149	14.157	13.196	14.981
10	16.111	15.273	14.326	13.358	12.433	-
30	14.744	13.967	13.080	12.124	11.274	13.117
100	13.784	13.057	12.227	11.257	10.464	-

(b) Pined-free

Nfgm	Donnell	Reissner	Sanders	Novozhilov	Teng	ABAQUS
0	53.503	51.206	48.590	45.353	42.515	-
0.5	46.333	44.310	41.926	39.061	36.369	40.005
1	42.211	40.364	38.066	35.405	32.911	-
5	34.929	33.231	31.173	28.929	26.851	27.511
10	32.788	31.133	29.127	26.940	24.910	-
30	30.060	28.469	26.592	24.565	22.692	26.173
100	28.437	26.907	25.113	23.092	21.297	-

(c) Fixed-fixed

Nfgm	Donnell	Reissner	Sanders	Novozhilov	Teng	ABAQUS
0	62.394	59.535	55.898	51.359	47.706	-
0.5	54.619	52.073	48.751	44.683	41.394	46.194
1	50.049	47.651	44.442	40.528	37.379	-
5	40.817	38.798	36.163	32.828	30.199	35.518
10	38.303	36.293	33.664	30.464	27.912	-
30	35.049	33.124	30.706	27.715	25.354	29.172
100	33.026	31.186	28.896	26.058	23.798	-

(d) Pined-pined

Nfgm	Donnell	Reissner	Sanders	Novozhilov	Teng	ABAQUS
0	62.222	59.439	56.424	52.941	49.964	-
0.5	54.245	51.803	49.154	46.062	43.436	47.318
1	49.540	47.284	44.820	41.833	39.350	-
5	40.306	38.453	36.399	33.914	31.850	35.995
10	37.934	36.162	34.193	31.856	29.900	-
30	34.832	33.204	31.258	29.078	27.212	30.818
100	32.877	31.340	29.484	27.425	25.605	-

Table 12 Comparison of the tenth frequency obtained by different theories and solid elements for various Nfgms

Nfgm	Donnell	Reissner	Sanders	Novozhilov	Teng	ABAQUS
0	121.086	119.923	119.500	119.488	119.524	119.553
5	79.655	77.294	76.854	76.331	76.549	76.804
30	70.607	68.306	67.251	66.910	67.007	67.111

Table 14 The effect of the number of stiffeners on fundamental frequencies obtained by different shell theories

Nfgm	Donnell	Reissner	Sanders	Novozhilov	Teng	ABAQUS
			NO. STR = 10			
1	36.689	36.358	36.283	36.245	36.245	36.301
8	26.122	25.884	25.832	25.793	25.798	25.800
100	22.716	22.510	22.464	22.428	22.435	22.459
			NO. STR = 15			
1	31.119	30.833	30.746	30.724	30.730	30.528
8	22.137	21.933	21.867	21.853	21.860	21.869
100	19.288	19.109	19.045	19.037	19.045	19.003
			NO. STR = 20			
1	27.885	27.625	27.534	27.522	27.531	27.541
8	19.821	19.633	19.564	19.562	19.568	19.562
100	17.300	17.135	17.073	17.073	17.078	17.036
			NO. STR = 25			
1	25.725	25.478	25.388	25.386	25.394	25.388
8	18.265	18.088	18.040	18.032	18.035	18.049
100	15.964	15.808	15.762	15.753	15.758	15.694
			NO. STR = 30			
1	24.159	23.922	23.854	23.835	23.842	28.855
8	17.122	16.954	16.896	16.886	16.898	16.896
100	14.979	14.827	14.780	14.764	14.777	14.781
			NO. STR = 35			
1	22.958	22.724	22.643	22.625	22.620	22.639
8	16.225	16.048	16.001	15.990	15.978	15.982
100	14.203	14.042	14.005	13.987	13.978	14.021
			NO. STR = 40			
1	22.000	21.736	21.688	21.665	21.643	21.671
8	15.480	15.294	15.256	15.238	15.218	15.249
100	13.549	13.403	13.378	13.305	13.325	13.293

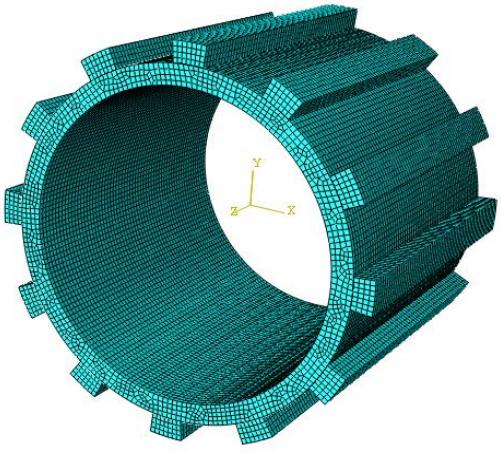

Fig. 6 Three dimensional mesh of a stiffened cylindrical shell

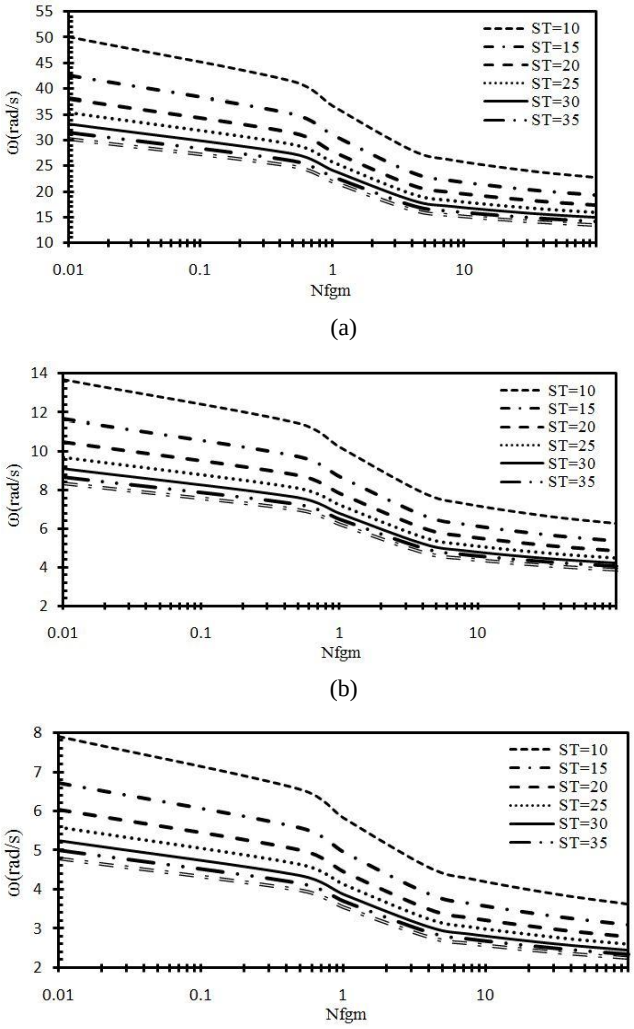

(a)

(b)

(c)

Fig. 7 The effect of the number of stiffeners on natural frequency for different length-to-radius ratios: (a) L/R = 1; (b) L/R = 3; (c) L/R = 6

In the next section, we define 4 different cases of the problem based on shell boundary conditions (fixed-free, pined-free, fixed-fixed, and pined-pined). The results are shown in Tables 13(a)-(d).

According to Tables 13(a)-(d), it is obvious that the theories are also sensitive to support conditions. Among the discussed theories, the Novozhilov and Reissner theories have the maximum and the minimum sensitivity to support conditions, respectively. Among the support conditions, fixed-fixed, pinned-free, fixed-free, and pined-pined types have the maximum influence, respectively, on the differences between the theories. According to Tables 13(a)-(d), it can be observed that the frequency values obtained from Sanders's theory have the maximum conformity with the values obtained from 3D analysis, and in comparison with the other shell theories studied in this research, they have a higher precision in the free vibration analysis of cylindrical shells.

3.2.2 Stiffened cylindrical shells

In this part of the problem, by considering the geometry

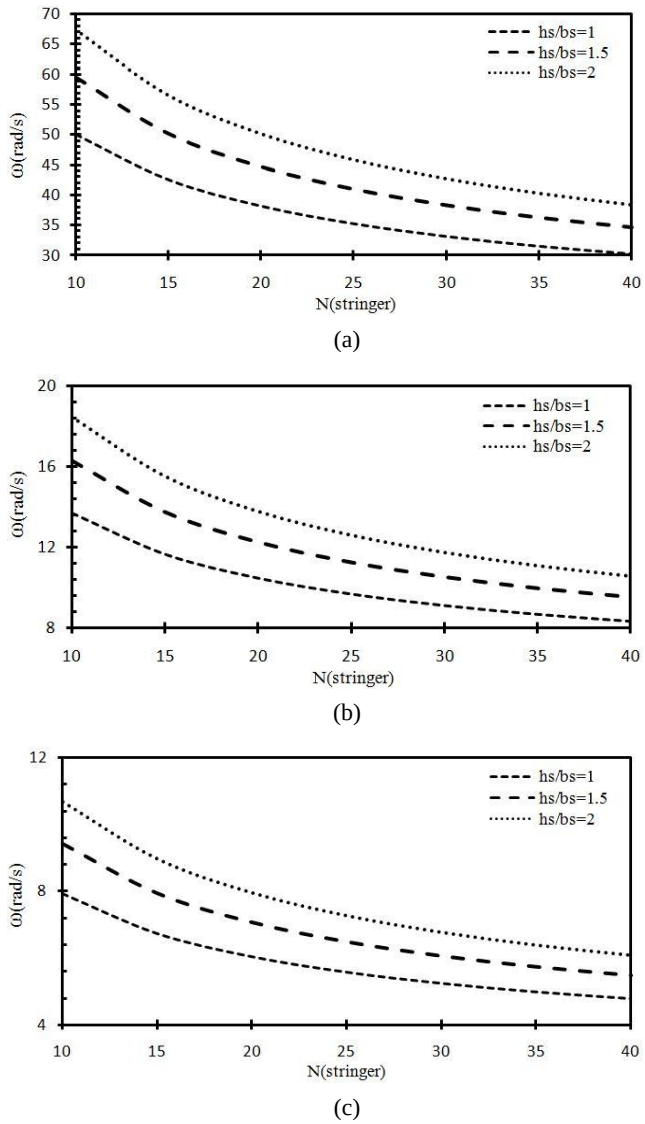

Fig. 8 The effect of the size of stiffeners on fundamental frequency for Nfgm = 0 for different length-to-radius ratios: (a) L/R = 1; (b) L/R = 3; (c) L/R = 6

introduced in the previous Section 3.2.1, the shell is strengthened using longitudinal reinforcement. The volume of the stiffeners is equal to 0.1 of the shell volume. Boundary conditions are of pined-pined type and the stiffener height to width ratio is equal to 1. The effect of the number of stiffeners on the difference between frequency values obtained from different theories are investigated. The obtained results are shown in Table 14. The accuracy of free vibration analyses of simply supported stiffened FGM cylindrical shells was examined comparing the results with those obtained by finite element software ABAQUS (Fig. 6) and using solid elements.

This table shows that the number of stiffeners does not have a significant effect on the values obtained from different theories. In other words, the results obtained by various shell theories are not very sensitive to the stiffeners and their numbers. The results obtained by Sanders's theory are shown in Figs. 7(a)-(c) for different numbers of stiffener and three different length-to-radius ratios of the shell.

As can be seen in Fig. 7 increasing the number of stiffeners reduces the frequency of the cylindrical shell and this is the same for all Nfgms. Moreover, the mentioned process has an identical trend for the three different length-to-radius ratios. Then, the effect of the stiffener's three height-to-width ratios of 1, 1.5, and 2 with the same stiffener volume mentioned above on natural frequency has been investigated. The shell has three length-to-radius ratios of 1, 3, and 6. The results are presented in Figs. 8(a)-(c) and 9(a)-(c) for two Nfgms of 0 and 5, respectively.

As can be seen in Figs. 8(a)-(c) and 9(a)-(c), by increasing the height-to-width ratio of the stiffeners for two Nfgms and different numbers of stiffeners, the frequency of the cylindrical shell increases.

4. Conclusions

In this study, the free vibration analyses of FGM cylindrical shells were investigated. In order to obtain the results, the shell was divided into several closed strips with their nodal lines in the circumferential direction. The governing equations were derived based on first-order shear deformation theory which accounts for through thickness shear flexibility. Displacements and rotations in the shell middle surface were approximated by combining polynomial functions in the meridional direction and truncated Fourier series using an appropriate number of harmonic terms in the circumferential direction. Different systems of equations were used to model the vibration behavior of circular cylindrical shells. In this study, Donnell, Reissner, Sanders, Novozhilov, and Teng's theories were used to find natural frequencies. A parametric study including various shell geometries, different boundary conditions, and various functionally graded materials with and without stiffeners was carried out. As the result, based on the presented results, the reader comprehends the importance of choosing a shell theory in designing thin-walled cylindrical shells. The numerical results support the following conclusions:

(1) All of the assumptions in this paper result in a reasonable accuracy for different shells and materials in the presence or absence of stiffeners.
(2) Among the theories which have been selected in this study, Sanders and Teng's theories had the best results, because they have the maximum conformity with the values obtained from 3D analysis.
(3) The results revealed that changing of thickness had the maximum effect on the difference of the frequencies obtained from the five discussed theories.
(4) The number of stiffeners did not have a significant effect on the values obtained from different theories.

References

Chaht, F.L., Kaci, A., Houari, M.S.A., Tounsi, A., Bég, O.A. and Mahmoud, S.R. (2015), "Ending and buckling analyses of functionallyw graded material (FGM) size-dependent nanoscale

beams including the thickness stretching effect", *Steel Compos. Struct., Int. J.*, **18**(2), 425-442.

Cinefra, M., Belouettar, S., Soave, M. and Carrera, E. (2010), "Variable kinematic models applied to free-vibration analysis of functionally graded material shells", *Eur. J. Mech.- A/Solids*, **29**(6), 1078-1087.

Civalek, Ö. (2017), "Vibration of laminated composite panels and curved plates with different types of FGM composite constituent", *Compos. Part B*, **122**, 89-108.

Damnjanovic, E., Marjanovic, M. and Danilovic, M.N. (2017), "Free vibration analysis of stiffened and cracked laminated composite plate assemblies using shear-deformable dynamic stiffness elements", *Compos. Struct.*, **180**, 723-740.

Donnell, L.H. (1934), Stability Of Thin-walled Tubes Under Torsion, NACA Report; CA, United States.

Duc, D.D. (2016), "Nonlinear thermal dynamic analysis of eccentrically stiffened S-FGM circular cylindrical shells surrounded on elastic foundations using the Reddy's third-order shear deformation shell theory", *Eur. J. Mech.- A/Solids*, **58**, 10-30.

Farid, M., Zahedinejad, P. and Malekzadeh, P. (2010), "Three-dimensional temperature dependent free vibration analysis of functionally graded material curved panels resting on two-parameter elastic foundation using a hybrid semi-analytic, differential quadrature method", *Mater. Des.*, **31**(1), 2-13.

Frikha, A., Wali, M., Hajlaoui, A. and Dammak, F. (2016), "Dynamic response of functionally graded material shells with a discrete double directors shell element", *Compos. Struct.*, **154**, 385-395.

Ganapathi, M. (2007), "Dynamic stability characteristics of functionally graded materials shallow spherical shells", *Compos. Struct.*, **79**(3), 338-343.

Jagtap, K.R., Lal, A. and Singh, B.N. (2011), "Stochastic nonlinear free vibration analysis of elastically supported functionally graded materials plate with system randomness in thermal environment", *Compos. Struct.*, **93**(12), 3185-3199.

Jin, G., Shi, S., Su, Z., Li, S. and Liu, Z. (2015), "A modified Fourier–Ritzapproach for free vibration analysis of laminated functionally graded shallow shells with general boundary conditions", *Int. J. Mech. Sci.*, **93**, 256-269.

Khalili, S.M.R. and Mohammadi, Y. (2012), "Free vibration analysis of sandwich plates with functionally graded face sheets and temperature-dependent material properties: A new approach", *Eur. J. Mech.- A/Solids*, **35**, 61-74.

Khayat, M., Poorvies, D. and Moradi, S. (2016a), "Buckling of Thick Deep Laminated Composite Shell of Revolution under Follower Forces", *Struct. Eng. Mech., Int. J.*, **58**(1), 59-91.

Khayat, M., Poorvies, D., Moradi, S. and Hemmati, M. (2016b), "Buckling analysis of laminated composite cylindrical shell subjected to lateral displacement-dependent pressure using semi-analytical finite strip method", *Steel Compos. Struct., Int. J.*, **22**(2), 301-321.

Khayat, M., Poorvies, D. and Moradi, S. (2017a), "Buckling analysis of functionally graded truncated conical shells under external displacement-dependent pressure", *Steel Compos. Struct., Int. J.*, **23**(1), 1-16.

Khayat, M., Poorvies, D. and Moradi, S. (2017b), "Semi-Analytical Approach in Buckling Analysis of Functionally Graded Shells of Revolution Subjected to Displacement Dependent Pressure", *J. Press. Vessel Technol.*, **139**.

Lee, H.W. and Kwak, M.K. (2015), "Free vibration analysis of a circular cylindrical shell using the Rayleigh–Ritz method and comparison of different shell theories", *J. Sound Vib.*, **353**(29), 344-377.

Loy, C.T., Lam, K.Y. and Reddy, J.N. (1999), "Vibration of functionally gradedcylindrical shells", *Int. J. Mech. Sci.*, **41**, 309-324.

Mahamood, R.M. and Akinlabi, E.T. (2012), "Functionally Graded Material: An Overview", *Proceedings of the World Congress on Engineering*, London, UK.

Mahmoud, S.R. and Tounsi, A. (2017), "A new shear deformation plate theory with stretching effect for buckling analysis of functionally graded sandwich plates", *Steel Compos. Struct., Int. J.*, **24**(5), 569-578.

Naghsh, A., Saadatpour, M.M. and Azhari, M. (2015), "Free vibration analysis of stringer stiffened general shells of revolution using a meridional finite strip method", *Thin-Wall. Struct.*, **94**, 651-662.

Nanda, N. and Sahu, S.K. (2012), "Free vibration analysis of delaminated composite shells using different shell theories", *Int. J. Press. Vessels Piping*, **98**, 111-118.

Novozhilov, V.V. (1964), *The Theory Of Thin Elastic Shells*, P. Noordhoff, Ltd., Groningen, The Netherlands.

Patel, B.P., Gupta, S.S., Loknath, M.S. and Kadu, C.P. (2005), "Free vibration analysis of functionally graded elliptical cylindrical shells using higher-order theory", *Compos. Struct.*, **69**, 259-270.

Qin, X.C., Dong, C.Y., Wang, F. and Qu, X.Y. (2017), "Static and dynamic analyses of isogeometric curvilinearly stiffened plates", *Appl. Math. Model.*, **45**, 336-364.

Rajasekaran, S. (2013), "Free vibration of centrifugally stiffened axially functionally graded tapered Timoshenko beams using differential transformation and quadrature methods", *Appl. Math. Model.*, **37**(6), 4440-4463.

Reissner, E. (1941), "A new derivation of the equations for the deformation of elastic shells", *Am. J. Math*, **63**,177-188.

Sanders, J.L. (1959), An Improved First-approximation Theory For Thin Shells; NACA Report, CA, United States.

Shahba, A. and Rajasekaran, S. (2012), "Free vibration and stability of tapered Euler–Bernoulli beams made of axially functionally graded materials", *Appl. Math. Model.*, **36**(7), 3094-3111.

Shahba, A., Attarnejad, R., Marvi, M.T. and Hajilar, S. (2011), "Free vibration and stability analysis of axially functionally graded tapered Timoshenko beams with classical and non-classical boundary conditions", *Compos. Part B*, **42**(4), 801-808.

Sofiyev, A.H. (2010), "The buckling of FGM truncated conical shells subjected to combined axial tension and hydrostatic pressure", *Compos. Struct.*, **92**, 488-498.

Su, Z., Jin, G. and Ye, T. (2014), "Free vibration analysis of moderately thick functionally graded open shells with general boundary conditions", *Compos. Struct.*, **117**, 169-186.

Teng, J.G. and Hong, T. (1998), "Nonlinear thin shell theories for numerical buckling predictions", *Thin-Wall. Struct.*, **31**, 89-115.

Tornabene, F. (2009), "Free vibration analysis of functionally graded conical, cylindrical shell and annular plate structures with a four-parameter power-law distribution", *Comput. Methods Appl. Mech. Eng.*, **198**, 2911-2935.

Tornabene, F. and Viola, E. (2009), "Free vibration analysis of functionally graded panels and shells of revolution", *Meccanica*, **44**(3), 255-281.

Tornabene, F., Fantuzzi, N. and Bacciocchi, M. (2014), "Free vibrations of free-form doubly-curved shells made of functionally graded materials using higher-order equivalent single layer Theories", *Compos. Part B: Eng.*, **67**, 490-509.

Tornabene, F., Brischetto, S., Fantuzzi, N. and Viola, E. (2015), "Numerical and exact models for free vibration analysis of cylindrical and spherical shell panels", *Compos. Part B*, **81**, 231-250.

Tornabene, F., Fantuzzi, N. and Bacciocchi, M. (2016), "The GDQ method for the free vibration analysis of arbitrarily shaped laminated composite shells using a NURBS-based iso-geometric approach", *Compos. Struct.*, **15**, 190-218.

Torki, M.E., Kazemi, M.T., Haddadpour, H. and Mahmoudkhani, S. (2014), "Dynamic stability of cantilevered functionally graded cylindrical shells under axial follower forces", *Thin-Wall. Structures*, **79**, 138-146.

Wali, M., Hentati, T. and Dammak, F. (2015), "Free vibration analysis of FGM shell structures with a discrete double directors shell element", *Compos. Struct.*, **125**, 295-303.

Zghal, S., Frikha, A. and Dammak, F. (2018), "Free vibration analysis of carbon nanotube-reinforced functionally graded composite shell structures'', *Appl. Math. Model.*, **53**, 132-155.

CC